# Effects of Squealer Rim Height on Aerodynamic Losses Downstream of a High-Turning Turbine Rotor Blade

*Sang Woo Lee, Byoung Joo Chae*
*School of Mechanical Engineering, Kumoh National Institute of Technology*
*1 Yangho-dong, Gumi, Gyeongbuk 730-701, Korea*

*Keywords: Turbine Rotor Blade, Squealer Rim Height, Aerodynamic Loss, Tip Leakage Vortex*

## Abstract

The effects of squealer rim height on three-dimensional flows and aerodynamic losses downstream of a high-turning turbine rotor blade have been investigated for a typical tip gap-to-chord ratio of $h/c$ = 2.0%. The squealer rim height-to-chord ratio is changed to be $h_{st}/c$ = 0.00 (plane tip), 1.37, 2.75, 5.51, and 8.26%. Results show that as $h_{st}/c$ increases, the tip leakage vortex tends to be weakened and the interaction between the tip leakage vortex and the passage vortex becomes less severe. The squealer rim height plays an important role in the reduction of aerodynamic loss when $h_{st}/c \leq 2.75\%$. In the case of $h_{st}/c \geq 5.51\%$, higher squealer rim cannot provide an effective reduction in aerodynamic loss. The aerodynamic loss reduction by increasing $h_{st}/c$ is limited only to the near-tip region within a quarter of the span from the casing wall.

## Introduction

The clearance gap between the tip of a turbine rotor blade and the adjacent stationary casing wall forms a narrow flow passage. Due to the presence of pressure difference between the pressure and suction sides of the blade, there exists a strong leakage flow through the tip gap. Interacting with main passage flow, it rolls into a tip leakage vortex along the blade suction side. This undesirable tip leakage flow delivers not only an aerodynamic loss penalty but also an additional thermal loading to the blade tip. Total pressure losses at the exit of a turbine rotor stage are known to be directly proportional with the tip gap height. The interaction of the tip leakage flow with the main passage flow causes significant aerodynamic loss and results in stage inefficiency.

Many investigations have been conducted on the tip leakage flow development and aerodynamic loss generation through the tip gap. Sjolander and Amrud[1] investigated the effect of leakage flow on the blade loading of a linear cascade. They showed the existence of separation lines on the cascade endwall and of separation bubbles on the tip surface caused by the leakage flow. Yamamoto[2] measured the leakage flow in a linear cascade and discussed the interactions of the leakage flow with the passage vortex at design incidence. Bindon[3] investigated the detailed development of tip clearance loss from the leading edge of a linear turbine cascade and quantified the contributions made by mixing, internal gap shear flow and endwall/secondary flow. He also suggested a conceptual flow model in the tip gap region. Moore et al.[4] investigated the effect of Reynolds number on flow and heat transfer in turbine tip gaps for an idealized two-dimensional tip gap geometry, and found a large separation off the sharp edge of the blade tip corner at high Reynolds numbers. Yamamoto[5] discussed the mechanism of three-dimensional flow and of the associated losses occurring near the tip endwall region of a linear turbine cascade with various tip gaps and incidences. Bindon and Morphis[6] found that radiusing and contouring the blade at gap inlet eliminate the tip-inlet separation bubble and reduce internal gap loss but create higher mixing loss to give almost unchanged overall loss coefficients when compared with the simple sharp-edged plain-tip blade. Tallman and Lakshminarayana[7] carried out a numerical simulation of plane-tip leakage flows with the variation of the tip gap height, and discussed various flow physics related to the tip leakage flows.

A squealer tip provides an enclosed cavity over the turbine rotor blade tip surface. It is known that the squealer tip increases resistance to tip leakage to reduce the flow rate through the tip gap and protects the tip surface from full thermal impact of high temperature leakage flow. It is also thought to act as a labyrinth seal between the casing wall and the blade tip. With reducing the risk of catastrophic failure of its rubs into the casing wall, the squealer tip allows for a smaller tip gap height than the plane tip. Heyes et al.[8] reported effects of using plain tips, suction-side squealer tips and pressure-side squealer tips. They found that the use of the squealer tips, particularly suction-side squealer tips can provide a benefit over the plane tip. Ameri et al.[9] performed three-dimensional simulations of the flow and heat transfer over a turbine blade with two squealer tips of 2 and 3% recesses, and found two dominant vortical structures in the recess region and no significant effect on efficiency due to the recessed tip. Azad et al.[10] measured detailed heat transfer coefficients and static pressure distributions on the squealer tip surface with a 3.77% recess, and found that the squealer tip blade provides lower overall heat transfer coefficients compared to the plane tip blade. Ameri[11] conducted experimental and computational works on the heat transfer and flow on the blade tip equipped with a

mean camber-line squealer, and showed that the sharp-edge camber-line squealer works better than the radiused-edge tip in reducing tip leakage flow and tip heat transfer. Camci et al.[12] found that suction-side partial squealers are aerodynamically superior to pressure-side ones and channel arrangements, and are capable of reducing the stage exit total pressure defect associated with the tip leakage flow to a significant degree. Key and Arts[13] compared plane-tip leakage flow with squealer-tip one at high-speed conditions and showed that the squealer tip provides a significant decrease in velocity through the tip gap.

As mentioned above, effects of various kinds of squealer tips on heat transfer and aerodynamic characteristics were documented by many investigators. However, there seems to be no systematic study which deals with effects of squealer rim height on aerodynamics even for the blade tip surrounded by a full-length squealer rim. In this study, the effects of the squealer rim height on the three-dimensional flow and aerodynamic loss generation have been investigated downstream of a high-turning rotor blade equipped with various full-length squealer rims.

## Experimental Apparatus and Procedure

### Linear Cascade Wind Tunnel

As shown in Fig. 1, the cascade wind tunnel comprises an open-circuit type wind tunnel, an inlet duct, a linear turbine cascade with a tip clearance gap, and an exhaust duct in turn. The open-circuit type wind tunnel has a cross section of 0.6m × 0.4m, and the inlet duct has a cross section of 0.42m × 0.32m. The flow coming out from the wind tunnel is developing to a turbulent boundary-layer flow on the top and bottom walls of the inlet duct, after passing a trip wire and a sand paper. The trip wire has its diameter of 1.8mm.

As shown in Fig. 1, the linear turbine cascade has six large-scale turbine blades, and its entrance is located 1.2 m downstream of the wind tunnel. The six large-scale turbine blades are fabricated based on the mid-span profile of a high-turning first-stage turbine rotor blade for power generation, and they are made of aluminum. As listed in Fig. 2, the chord length, c, axial chord, b, pitch, p, and span, s, of the large-scale cascade are 217.8mm, 196.0mm, 151.6mm, and 320.0mm, respectively. The span is determined, based on the aspect ratio of original blade of s/c = 1.47. The blade profile used in this study is reported by Jun14).

As can be seen in Fig. 1, the central four blades can be inserted into the indents machined on the bottom wall, and thus they have a tip gap height, h, on the top end (Fig. 2). On the other hand, the blades #1 and #6 are attached to the top and bottom walls with no tip gap. For static pressure measurements along the blade surface, 22 pressure-sensing holes of 1.2mm in diameter are drilled on the surface of the blade #3. In the xyz coordinates (Fig. 2), x, y, and z are in the axial, pitch-wise and span-wise directions of the cascade.

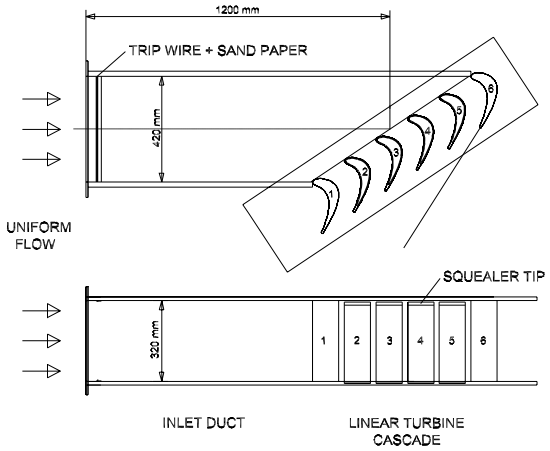


Fig. 1 Overall view of cascade wind tunnel

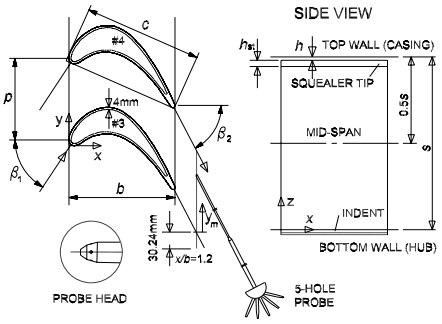


| | |
|---|---|
| Number of blades | 6 |
| Chord length ($c$) | 217.8 mm |
| Axial chord ($b$) | 196.0 mm |
| Pitch ($p$) | 151.6 mm |
| Span ($s$) | 320.0 mm |
| Blade inlet angle ($\beta_1$) | 56.4 deg |
| Blade outlet angle ($\beta_2$) | -62.6 deg |

Fig. 2 Turbine rotor blade with a squealer tip

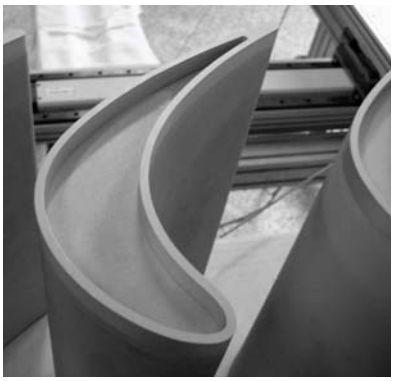

Fig. 3 Photograph of a tested squealer tip ($h_{st}/c$ = 5.51%)

### Squealer Tip

The squealer tip used in this study is shown in Fig. 2. It is surrounded by a full-length squealer rim. The squealer rim is 4mm in width, and its height, hst, is changed to be 0mm, 3mm, 6mm, 12mm, and 18mm.

Each squealer rim is attached on the plane tip surface with glue. The depth of insertion into the indent can be adjusted in order to maintain the tip gap-to-chord ratio, h/c, to be fixed as 2.0% regardless of the squealer rim height. Fig. 3 shows the blade tips equipped with the full-length squealer of hst = 12 mm.

**Five-Hole Probe**

A cone-type five-hole probe of 3.18 mm (0.125 inch) in head diameter, custom-made by United Electric Controls, is used to measure three-dimensional flow fields (Fig. 2). The five-hole probe, which is also used by Lee et al.[15], has a straight probe stem of about 1.1 m in total length, and its reinforced portion is 6.35 mm (0.25 inch) in diameter and 0.86 m long. The probe tip shape is the same as that of its DC125 model.

**Instrumentation**

All the measurements are controlled by a personal computer (Samsung, Pentium 4) equipped with plug-in boards such as a Multi-Function I/O Board (NI, PCI-MIO-16E-4) and a Digital I/O board (NI, PCI-6503). Measured pressures are transformed into DC voltages by a high-accuracy differential pressure transducer (MKS, Type 120AD-00010-R-EB) and power supply/readout (MKS, Type 501B). The DC voltages are sampled by a 12-bit A-D converter in the Multi-Function DI/O Board, and transferred into the computer. A three-dimensional automatic probe traverse system used for probing has linear motion guides (Samik, SAR1615T), stepping motors (Oriental Motor, UPH599-A), and stepping motor drivers (Oriental Motor, UDX5114). This traverse system is controlled by six-channel digital-out pulses from the Multi-Function I/O Board. A 20-channel pressure scanning box (Furness Controls, FC091 MKII) is used for sequential switching of pressure-sensing holes of the five-hole probe. This is controlled by BCD pulse inputs which are provided by the Digital I/O Board. The whole measurement system is controlled in a proper sequence by an instrumentation program based on LabVIEW software (NI, Version 7.0).

## Experimental Conditions and Uncertainties

Free-stream velocity in the inlet duct, $U_\infty$, is maintained at 15.0 m/s. The Reynolds number based on the free-stream velocity and the chord length, Re, is $2.09 \times 10^5$. At the location 1.5$c$ upstream of the cascade inlet, turbulent intensity level is about 0.3%, and boundary-layer thickness, displacement thickness, and momentum thickness are 44.7mm, 5.16mm, and 4.04mm, respectively. Throughout the present experiments, the tip gap-to-chord ratio is fixed as a typical value of $h/c$ = 2.0%, but the squealer rim height-to-chord ratio is changed to be $h_{st}/c$ = 0.00 (plane tip), 1.37, 2.75, 5.51, and 8.26%, which are equivalent to the squealer rim height-to-span ratio, $h_{st}/s$, of 0.00, 0.94, 1.88, 3.75, and 5.63%, respectively.

Static-pressure coefficient is generally defined in the following way.

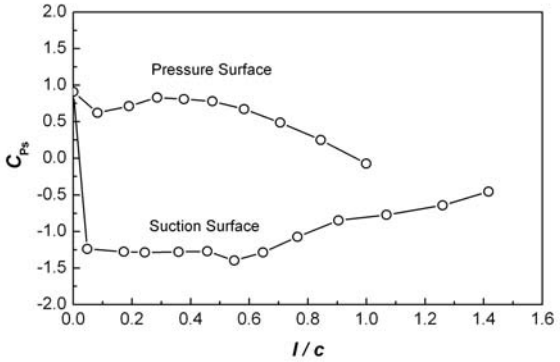


Fig. 4 Mid-span static-pressure coefficients along the blade surface

$$C_{Ps} = \frac{P_s - P_{s,0}}{\frac{1}{2}\rho U_\infty^2} \quad (1)$$

The static-pressure coefficients along the blade surfaces at the mid-span with no tip gap are presented in Fig. 4.

A downstream coordinate, $y_m$, introduced in Fig. 2 is in parallel with the $y$-axis and has its origin at the intersection of a line of $x/b$ = 1.2 with a line drawn from the trailing-edge center at the blade outlet angle. Three-dimensional flow fields are measured in the $y_m$-$z$ plane of $x/b$ = 1.2 as indicated in Fig. 2. The measurements are performed at 31 points from $y_m/p$ = -0.2 to 1.0 in the $y$-direction and at 27 points from the mid-span ($z/s$ = 0.5) to the top casing wall ($z/s$ = 0.5) in the $z$-direction.

A non-nulling data reduction program for five-hole probe based on Treaster and Yocum[16] is used to determine flow angles, total pressure, and static pressure from calibration data[17]. In order to minimize the effect of probe Reynolds number, calibration is performed at the same velocity as the present free-stream one. The five-hole probe is calibrated for both pitch and yaw angles in the range from –40 to +40 deg with an angle interval of 5 deg. Flow blockage can be minimized by aligning the five-hole probe as in Fig. 2.

The uncertainty intervals are evaluated with 95% confidence[18]. Uncertainties associated with the probe location are given by ±0.1 mm in both $y$- and $z$-directions. In pressure measurements, uncertainty is estimated to be ±0.7% of free-stream dynamic pressure. In the five-hole probe measurements, uncertainty intervals are calculated to be ±1.2 deg in the pitch and yaw angles and ±1.5% of $U_\infty$ in the velocity magnitude, in the absence of additional uncertainties resulted from local turbulence and velocity gradient. After completion of experiments, repeatability is checked for $h_{st}/c$ = 2.75%. The repeatability test shows that the difference in $\overline{C}_{Pt}$ falls within 2.0%, even though the tip leakage flow is highly turbulent with steep velocity gradient.

## Results and Discussion

### Three-Dimensional Flow Data

Detailed three-dimensional flow fields are measured at $x/b$ = 1.2 to understand the effect of $h_{st}/c$ on the downstream mean flow for $h/c$ = 2.0%. Additional flow data with no tip gap ($h/c$ = 0.0%.) are also collected for comparisons. Fig. 5 shows contours of velocity magnitude, $Q/U_\infty$, in the $y_m$-$z$ plane at $x/b$ = 1.2. Without tip gap (Fig. 5(a)), the deficit of $Q/U_\infty$ is found very small in comparison with those for $h/c$ = 2.0% (Figs. 5(b) - (d)). Regardless of $h_{st}/c$ for $h/c$ = 2.0%, the deficit of $Q/U_\infty$ is always found in three regions: a wake region behind the trailing edge near the mid-span; a passage vortex region; and a tip leakage flow region. The tip leakage flow region is located near the casing wall ($z/s$ = 1.0) and has the lowest velocity magnitude among the three regions. The passage vortex region found in the area between the tip leakage flow region and the mid-span has the largest extent regardless of $h_{st}/c$. In the case of the plane tip ($h_{st}/c$ = 0.0%), the tip leakage flow region has the largest velocity deficit and the widest area, as can be seen in Fig. 5(b). With the increment of $h_{st}/c$, the minimum value of $Q/U_\infty$ in the tip leakage flow region increases. As $h_{st}/c$ increases, not only the extent of the tip leakage flow region but also the area of the passage vortex region tends to decrease. Fig. 5 shows that higher squealer rim delivers lower velocity-magnitude deficit in the tip leakage flow region due to the weaker interaction between the leakage and main passage flows, which implies that higher squealer rim has an effect to reduce the tip leakage mass flow rate.

Fig. 6 demonstrates secondary flows in the $y$-$z$ plane at $x/b$ = 1.2. The velocity vectors are drawn based on the $y$- and $z$-directional velocity components subtracted by the corresponding mid-span ones, respectively. In the case of no tip gap (Fig. 6(a)), there exists only a well-organized counter-clockwise vortex called a passage vortex. In the case of $h/c$ = 2.0% (Figs. 6(b) – (d)), however, two distinct vortices are found. A clockwise vortex near the casing wall is called a tip leakage vortex. This arises from the interaction of the jet-like leakage flow coming out of the tip gap with the main passage flow, along the suction-side tip corner. The secondary flow resulted from tip leakage is confined only near the casing wall, but its magnitude is much larger than that from the passage vortex. The tip leakage vortex in the case of the plane tip ($h_{st}/c$ = 0.0%) is found strongest among the three cases for $h/c$ = 2.0% in Fig. 6. It is also revealed that higher $h_{st}/c$ results in weaker intensity and smaller occupying area of the tip leakage vortex, even though the tip gap remains constant at $h/c$ = 2.0%. A close examination shows that as $h_{st}/c$ decreases from 2.75 (Fig. 6(d)) to 0.0 (Fig, 6(b)) in the case of $h/c$ = 2.0%, the passage vortex center moves not only in the positive $y$-direction but also toward the casing wall. As a result, the passage vortex comes closer to the tip leakage vortex, which stimulates the interaction between the two counter-rotating vortices.

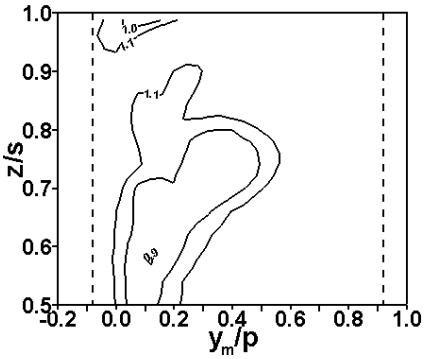


(a) $h/c$ = 0.0% (no tip gap)

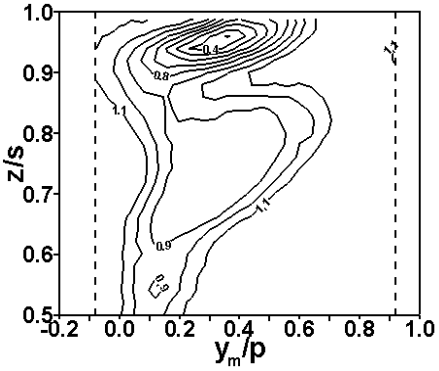


(b) $h/c$ = 2.0% and $h_{st}/c$ = 0.0%

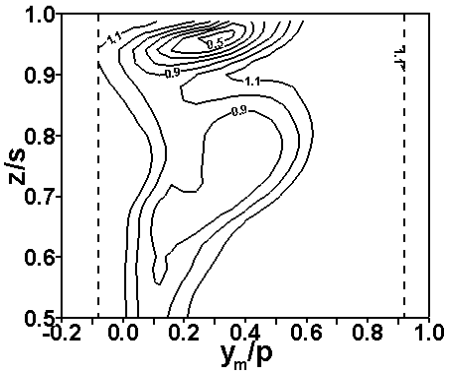


(c) $h/c$ = 2.0% and $h_{st}/c$ = 1.37%

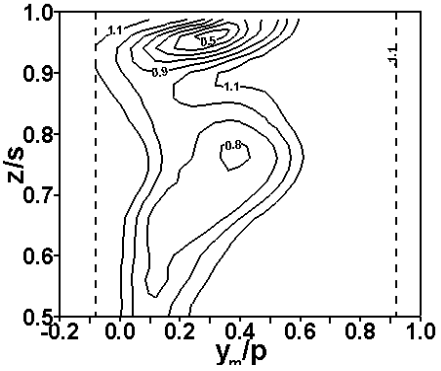


(d) $h/c$ = 2.0% and $h_{st}/c$ = 2.75%

Fig. 5 Contours of $Q/U_\infty$ at $x/b$ = 1.2

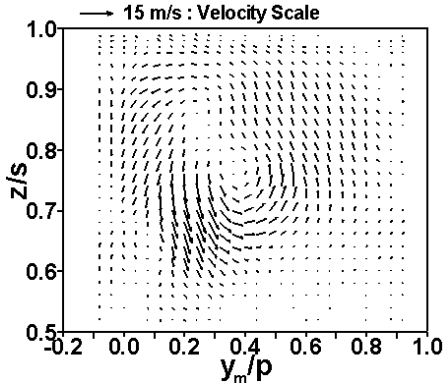


(a) $h/c$ = 0.0% (no tip gap)

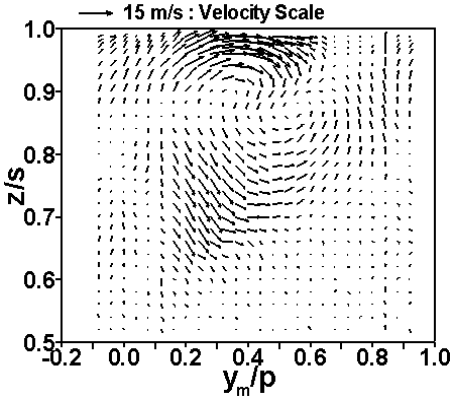


(b) $h/c$ = 2.0% and $h_{st}/c$ = 0.0%

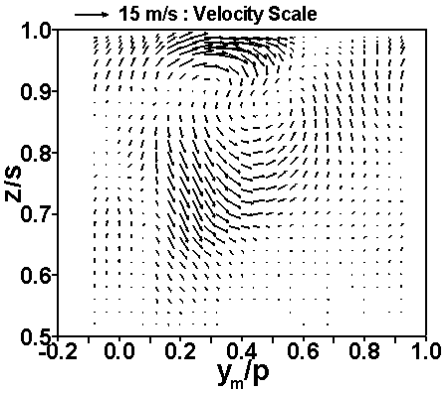


(c) $h/c$ = 2.0% and $h_{st}/c$ = 1.37%

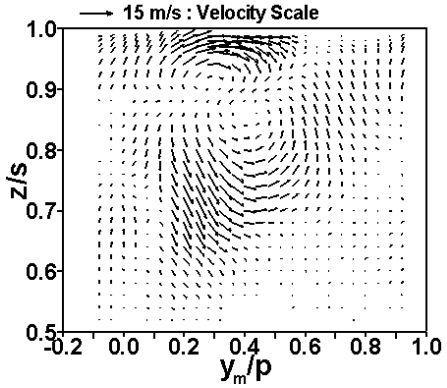


(d) $h/c$ = 2.0% and $h_{st}/c$ = 2.75%

Fig. 6 Secondary flows in the $y_m$-$z$ plane at $x/b$ = 1.2.

**Aerodynamic Losses**

Aerodynamic loss is a measure of total pressure deficit. The local total-pressure loss coefficient is defined in the following way.

$$C_{Pt} = \frac{P_{t,0} - P_t}{\rho U_\infty^2 / 2} \tag{2}$$

where $P_{t,0}$ is a reference total pressure measured at the inlet duct and $P_t$ denotes local total pressure measured in the $y_m$-$z$ plane at $x/b$ = 1.2. The total-pressure loss coefficient mass-averaged in the pitch-wise direction, $\overline{C}_{Pt,z}$, can be defined as follows.

$$\overline{C}_{Pt,z} = \frac{\int_0^p \rho U C_{Pt} dy_m}{\int_0^p \rho U dy_m} \tag{3}$$

The mass-averaged total-pressure loss coefficient all over the measurement plane, $\overline{C}_{Pt}$, can be obtained as in the following equation.

$$\overline{C}_{Pt} = \frac{\int_{0.5s}^{s} \int_0^p \rho U C_{Pt} dy_m dz}{\int_{0.5s}^{s} \int_0^p \rho U dy_m dz} \tag{4}$$

$\overline{C}_{Pt}$ can also be obtained by averaging $\overline{C}_{Pt,z}$ in the $z$-direction.

$$\overline{C}_{Pt} = \int_{0.5s}^{s} \overline{C}_{Pt,z} dz \tag{5}$$

Profile loss is defined as aerodynamic loss generated at the mid-span. Thus, the mass-averaged profile loss coefficient, $\left(\overline{C}_{Pt}\right)_P$, is the same as the total-pressure loss coefficient mass-averaged in the pitch-wise direction at the mid-span.

$$\left(\overline{C}_{Pt}\right)_P = \overline{C}_{Pt,z=0.5s} = \frac{\int_0^p (\rho U C_{Pt})_{z=0.5s} dy_m}{\int_0^p (\rho U)_{z=0.5s} dy_m} \tag{6}$$

The mass-averaged secondary loss coefficient, $\left(\overline{C}_{Pt}\right)_S$, is determined by subtracting $\left(\overline{C}_{Pt}\right)_P$ from $\overline{C}_{Pt}$.

$$\left(\overline{C}_{Pt}\right)_S = \overline{C}_{Pt} - \left(\overline{C}_{Pt}\right)_P \tag{7}$$

Contours of the total-pressure loss coefficient, $C_{Pt}$, in the $y_m$-$z$ plane at $x/b$ = 1.2 are presented in Fig. 7. In the case of no tip gap (Fig. 7(a)), aerodynamic loss is usually generated in the wake region behind the trailing edge near the mid-span and in the region where the passage vortex resides. In this case, the highest value of $C_{Pt}$ is found at the passage vortex center, which means that the passage vortex plays a

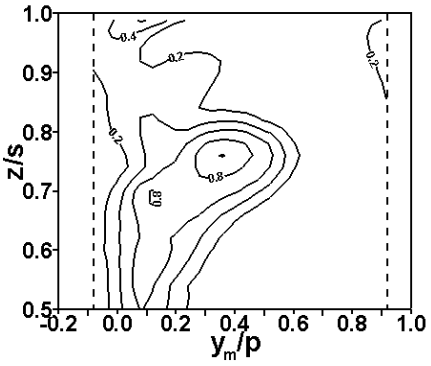


(a) $h/c$ = 0.0% (no tip gap)

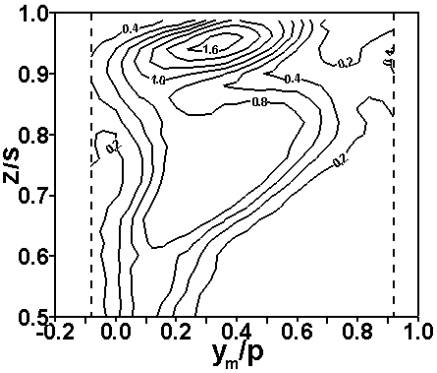


(b) $h/c$ = 2.0% and $h_{st}/c$ = 0.0%

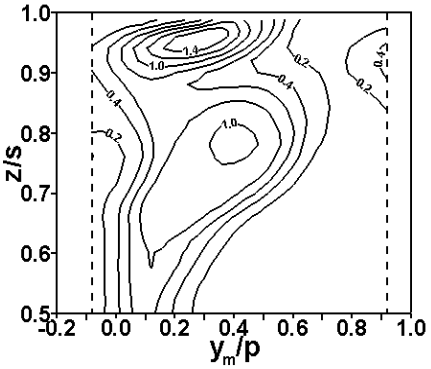


(c) $h/c$ = 2.0% and $h_{st}/c$ = 1.37%

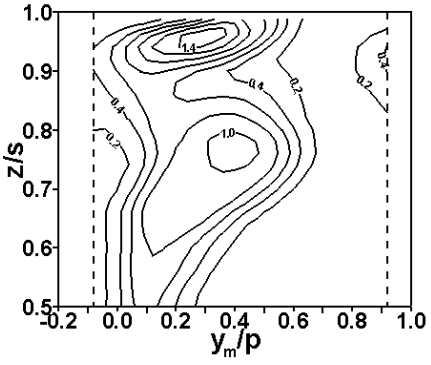


(d) $h/c$ = 2.0% and $h_{st}/c$ = 2.75%

Fig. 7 Contours of $C_{pt}$ at $x/b$ = 1.2

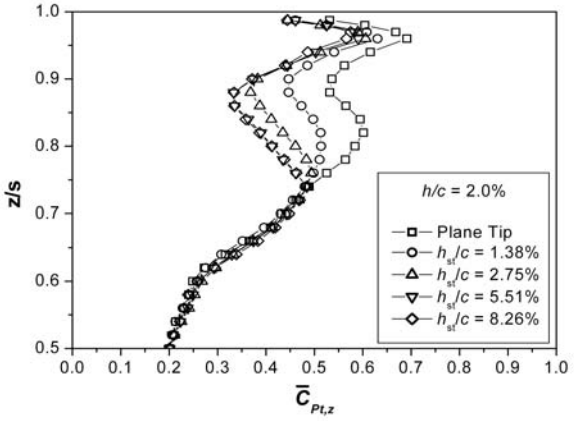


Fig. 8 Profiles of pitch-wise mass-averaged loss coefficient, $\overline{C}_{Pt,z}$, at $x/b$ = 1.2

key role to generate aerodynamic loss downstream of a turbine blade with no tip gap. Fig. 7 shows that aerodynamic loss in the case of $h/c$ = 2.0% (Figs. 7(b) - (d)) is much higher than that with no tip gap (Fig. 7(a)). For $h/c$ = 2.0%, $C_{Pt}$ has a higher value in the tip leakage flow region as well as in the mid-span wake region and in the passage vortex region. $C_{Pt}$ in the tip leakage flow region is highest among the three regions. This tip leakage loss may be originated mostly from the losses generated within the tip gap and from subsequent mixing of the leakage jet with the main passage flow. With increasing $h_{st}/c$ from 0.0% (plane tip) to 2.75%, not only the peak value of $C_{Pt}$ but also the area with higher $C_{Pt}$ in the tip leakage flow region tends to decrease. This is because in the case of higher $h_{st}/c$, there are lower leakage mass flow rate and its weaker interaction with the main passage flow. With the increment of $h_{st}/c$, the peak value of $C_{Pt}$ in the passage vortex region increases, but its area with higher $C_{Pt}$ decreases.

Profiles of the mass-averaged total-pressure loss *coefficient* in the pitch-wise direction, $\overline{C}_{Pt,z}$, for $h/c$ = 2.0% are presented in Fig. 8 as a function of $z/s$. In general, higher value of $h_{st}/c$ results in lower $\overline{C}_{Pt,z}$ especially in the range of $0.75 \le z/s \le 1.00$. However, differences in $\overline{C}_{Pt,z}$ among the various cases of $h_{st}/c$ are found to be minute in the range of $0.50 \le z/s \le 0.75$. In particular, $\overline{C}_{Pt,z}$ at the mid-pan, which is defined as $\left(\overline{C}_{Pt}\right)_P$ in Eq. (6), has nearly the same value of about 0.2 regardless of $h_{st}/c$. With the increment of $h_{st}/c$, the profile of $\overline{C}_{Pt,z}$ tends to approach that for $h_{st}/c$ = 8.26%. After all, the profile of $\overline{C}_{Pt,z}$ for $h_{st}/c$ = 5.51% almost coincides with that for $h_{st}/c$ = 8.26%. This fact means that when $h_{st}/c \ge$ 5.51%, increasing of $h_{st}/c$ has no effect in reducing aerodynamic loss.

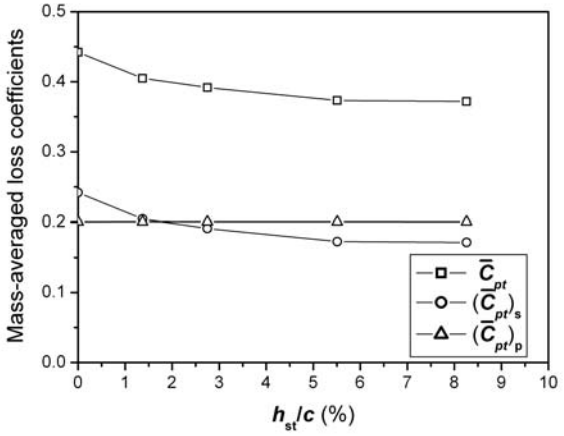


Fig. 9 Mass-averaged loss coefficients as a function of $h_{st}/c$ at $x/b$ = 1.2 for $h/c$ = 2.0%

As a whole, $\overline{C}_{Pt,z}$ has two peaks. The first peak, which has a maximum value of $\overline{C}_{Pt,z}$ across the span, is located in the tip leakage flow region. Regardless of $h_{st}/c$, its locations seem to be fixed at about $z/s$ = 0.95. On the contrary, the second peak shifts toward the mid-span as $h_{st}/c$ increases. When $h_{st}/c \geq 5.51\%$, the second one is finally positioned at about $z/s$ = 0.75. This elevation is nearly the same as that of the passage vortex center in the case of no tip gap (Fig. 6(a)). In the range of $0.50 \leq z/s \leq 0.75$, there are no noticeable differences among the profiles of $\overline{C}_{Pt,z}$ for $h/c$ = 2.0% while significant discrepancies are found in the range $0.75 \leq z/s \leq 1.00$. Therefore, it is concluded that the squealer rim height effect on aerodynamic loss is limited only to a quarter of the span from the casing wall. The results in the range $0.75 \leq z/s \leq 1.00$ also imply that higher squealer rim effectively reduces the secondary losses induced not only by the tip leakage flow but also generated from the interaction of the tip leakage flow with the passage vortex.

As discussed earlier in Fig. 6, with decreasing $h_{st}/c$, the passage vortex comes closer to the tip leakage vortex. This proximity between the two counter-rotating vortices stimulates the interaction with each other, and increases aerodynamic losses there in turn. This is why there is a large discrepancy in the $\overline{C}_{Pt,z}$-profiles in the range of $0.75 \leq z/s \leq 1.00$, and is also why at lower $h_{st}/c$, the second peak is closer to the first one.

Mass-averaged loss coefficients, $\overline{C}_{Pt}$, $\left(\overline{C}_{Pt}\right)_P$, and $\left(\overline{C}_{Pt}\right)_S$ *defined* in Eqs. (4), (6) and (7) are reported as a function of $h_{st}/c$ in Fig. 9. As $h_{st}/c$ increases, $\overline{C}_{Pt}$ decreases steeply when $h_{st}/c \leq 2.75\%$ and has a very mild slope when $h_{st}/c \geq 5.51\%$. On the other hand, $\left(\overline{C}_{Pt}\right)_P$ remains almost unchanged. As a result, $\left(\overline{C}_{Pt}\right)_S$ has the same trend as $\overline{C}_{Pt}$ does. As $h_{st}/c$ increases from 0% to 8.26%, $\overline{C}_{Pt}$ is reduced by about 16% of that for $h_{st}/c$ = 0%. The results in Fig. 9 lead to a valuable conclusion that the squealer rim height plays an important role in the reduction of aerodynamic loss when $h_{st}/c \leq 2.75\%$. In the case of $h_{st}/c \geq 5.51\%$, however, higher squealer rim cannot provide an effective reduction in aerodynamic loss.

## Conclusion

Effects of squealer rim height on the three-dimensional flow and aerodynamic loss downstream of a high-turning turbine rotor blade have been *investigated* for a typical tip gap-to-chord ratio, $h/c$, of 2.0%. The squealer rim height-to-chord ratios is changed to be $h_{st}/c$ = 0.00 (plane tip), 1.37, 2.75, 5.51, and 8.26%. Major findings are summarized as follows.

(1) As $h_{st}/c$ increases, the tip leakage vortex tends to be weakened, and the interaction between the tip leakage vortex and the passage vortex becomes less severe.

(2) With the increment of $h_{st}/c$, the mass-averaged total-pressure loss coefficient decreases noticeably meanwhile the mass-averaged profile loss coefficient remains almost unchanged.

(3) The aerodynamic loss reduction by increasing $h_{st}/c$ is limited only to the near-tip region within a quarter of the span from the casing wall.

(4) The squealer rim height plays an important role in the reduction of aerodynamic loss when $h_{st}/c \leq 2.75\%$. In the case of $h_{st}/c \geq 5.51\%$, however, higher squealer rim cannot provide an effective reduction in aerodynamic loss.

## References

1) Sjolander, S. A., and Amrud, K.K.: Effects of Tip Clearance on Blade Loading in a Planar Cascade of Turbine Blades, *ASME Journal of Turbomachinery*, **109**, 1987, pp. 237-245.
2) Yamamoto, A.,: Interaction Mechanisms Between the Tip Leakage Flow and the Passage Vortex in a Linear Turbine Cascade, *ASME Journal of Turbomachinery*, **110**, 1988, pp. 329-338.
3) Bindon, J. P.: The Measurement and Formation of Tip Clearance Loss, *ASME Journal of Turbomachinery*, **111**, 1989, pp. 257-263.
4) Moore, J., Moore, J. G., Henry, G. S., and Chaudhry, U.: Flow and Heat Transfer in Turbine Tip Gaps, *ASME Journal of Turbomachinery,* **111**, 1989, pp. 301-309.
5) Yamamoto, A.: Endwall Flow/Loss Mechanisms in a Linear Turbine Cascade with Blade Tip Clearance, *ASME Journal of Turbomachinery,* **111**, 1989, pp. 264-275.
6) Bindon, J. P., and Morphis, G.: The Development of Axial Turbine Leakage Loss for Two Profiled Tip Geometries Using Linear Cascade Data,

*ASME Journal of Turbomachinery*, **114**, 1992, pp. 198-203.

7) Tallman, J., and Lakshminarayana, B.: Numerical Simulation of Tip Leakage Flows in Axial Flow Turbines, with Emphasis on Flow Physics: Part I-Effect of Tip Clearance Height, *ASME Journal of Turbomachinery*, **123**, 2001, pp. 314-323.
8) Heyes, F. J. G., Hodson, H. P. and Dailey, G. M.: The Effect of Blade Tip Geometry on the Tip Leakage Flow in Axial Turbine Cascades, *ASME Journal of Turbomachinery*, **114**, 1992, pp. 643-651.
9) Ameri, A. A., Steinthorsson, E., and Rigby, D. L.: Effect of Squealer Tip on Rotor heat Transfer and Efficiency, *ASME Journal of Turbomachinery*, **120**, 1998, pp. 753-759.
10) Azad, Gm. S., Han, J-C, and Boyle, R. J.: Heat Transfer and Flow on the Squealer Tip of a Gas Turbine Blade, *ASME Journal of Turbomachinery*, **122**, 2000, pp. 725-732.
11) Ameri, A.A.: Heat Transfer and Flow on the Blade Tip of a Gas Turbine Equipped with a Mean Camberline Strip, *ASME Journal of Turbomachinery*, **123**, 2001, pp. 704-708.
12) Camci, C., Dey, D., and Kavurmacioglu, L.: Aerodynamics of Tip Leakage Flows near Partial Squealer Rims in an Axial Flow Turbine Stage, *ASME Journal of Turbomachinery*, **127**, 2005, pp. 14-24.
13) Key, N., and Arts, T.: Comparison of Turbine Tip Leakage Flow for Flat Tip and Squealer Tip Geometries at High Speed Conditions, *ASME Journal of Turbomachinery*, **128**, 2006, pp. 213-220.
14) Jun, S. B.: Measurements of Endwall Heat (Mass) Transfer Coefficient in a Linear turbine Cascade Using Naphthalene Sublimation Technique, M.S. Thesis, Kumoh National Institute of Technology, 2000.
15) Lee, S. W., Joo, S. K., and Lee, J. S.: Flow Characteristics Inside Circular Injection Holes Normally Oriented to a Crossflow: Part II-Three-Dimensional Flow Data and Aerodynamic Loss, *ASME Journal of Turbomachinery*, **123**, 2001, pp. 274-280.
16) Treaster, A. L., and Yocum, A. M.: The Calibration and Application of Five-Hole Probes, *ISA Transactions*, **18**, 1979, pp. 23-34.
17) Lee, S. W., Kim, Y. B., and Lee, J. S.: Flow Characteristics and Aerodynamic Losses of Film-Cooling Jets with Compound Angle Orientations, *ASME Journal of Turbomachinery*, **119**, 1997, pp. 310-319.
18) Abernethy, R. B., Benedict, R. P., and Dowdell, R. B.: ASME measurement uncertainty, *ASME Journal of Fluids Engineering*, **107**, 1985, pp. 161-164.

**Nomenclature**

| | |
|---|---|
| $b$ | axial chord length, mm |
| $c$ | chord length, mm |
| $C_{Ps}$ | static-pressure coefficient (Eq. (1)) |
| $C_{Pt}$ | total-pressure loss coefficient (Eq. (2)) |
| $\overline{C}_{Pt}$ | mass-averaged total-pressure loss coefficient (Eq. (4)) |
| $\left(\overline{C}_{Pt}\right)_P$ | mass-averaged profile loss coefficient (Eq. (6)) |
| $\overline{C}_{Pt,z}$ | total-pressure loss coefficient mass-averaged in the pitch-wise direction (Eq. (3)) |
| $\left(\overline{C}_{Pt}\right)_S$ | mass-averaged secondary loss coefficient (Eq. (7)) |
| $h$ | tip gap height, mm |
| $h_{st}$ | squealer rim height, mm |
| $l$ | distance from the stagnation point along the blade surface, mm |
| $p$ | pitch of the cascade, mm |
| $P_s$ | local static pressure, Pa |
| $P_{s,0}$ | reference static pressure, Pa |
| $P_t$ | local total pressure, Pa |
| $P_{t,0}$ | reference total pressure, Pa |
| $Q$ | velocity magnitude( $\sqrt{U^2+V^2+W^2}$ ), m/s |
| Re | Reynolds number ($U_\infty c/\nu$) |
| $s$ | span of the turbine blade, mm |
| $U, V, W$ | $x, y, z$-directional velocities, m/s |
| $U_\infty$ | Inlet free-stream velocity, m/s |
| $x, y, z$ | cascade coordinates, mm (Fig. 2) |
| $y_m$ | $y$-directional coordinate at $x/b$ = 1.2 ( Fig. 2) |

Greek Characters

| | |
|---|---|
| $\nu$ | kinemetic viscosity of air,$m^2/s$ |
| $\rho$ | density of air, $kg/m^3$ |